PNAS

Supporting Information for

The autism-associated loss of δ-catenin functions disrupts social behavior

Hadassah Mendez-Vazquez[1,7], Regan L. Roach[1,7], Kaila Nip[2,7,8], Soham Chanda[2,3,4], Matheus F. Sathler[1], Tyler Garver[3], Rosaline A. Danzman[1], Madeleine C. Moseley[3], Jessica P. Roberts[3], Olivia N. Koch[1], Ava A. Steger[5], Rahmi Lee[1], Jyothi Arikkath[6], and Seonil Kim[1,2,3*]

[1]Department of Biomedical Sciences,
[2]Cellular and Molecular Biology Program,
[3]Molecular, Cellular and Integrative Neurosciences Program,
[4]Department of Biochemistry & Molecular Biology, Colorado State University, Fort Collins, CO, 80523.
[5]Rocky Mountain High School, Fort Collins, CO, 80526.
[6]Developmental Neuroscience, Munore-Meyer Institute, University of Nebraska Medical Center, Omaha, NE, 68198.
[7]These authors contribute equally.

[8]Current address: Department of Cellular and Integrative Physiology, University of Texas Health Science Center San Antonio, San Antonio, TX, 78229.

* Corresponding Authors: Seonil Kim.
Email: seonil.kim@colostate.edu

This PDF file includes:

Supporting text
Figures S1 to S11
Tables S1 to S7
SI References

Supporting text

Methods and Materials

Generation of δ-catenin G34S mice

δ-catenin G34S mice (RRID:MMRRC_050621-UCD) were generated by Dr. Jyothi Arikkath at UNMC Mouse Genome Engineering Core using the CRISPR-Cas9 technique (1). Human and mouse δ-catenin proteins both contain glycine 34, according to amino acid sequence analysis (**Fig. S10a**). The CRISPR-Cas9 reagents (sgRNA, Cas9 mRNA and the donor DNA template) were injected into zygotes derived from C57BL6/J mice. The sgRNA sequence was 5'-CCATTGGAGGTGTTTAA/GCC*TGG*-3' (the cleavage site is shown by "/" and the PAM sequence is in italics). The sgRNA is in antisense orientation, and it cleaved immediately downstream of the codon GGC (glycine 34) of the *δ-catenin* gene, yielding a double-strand break. Non-homologous end joining was used to repair the breaks, which resulted in the G34S mutation being inserted into the *δ-catenin* gene *in vivo*. The offspring were genotyped using PCR-RFLP followed by sequencing. The founder mouse was crossed with WT C57Bl6/J mice to create heterozygous δ-catenin G34S mice, which were subsequently used to make homozygous G34S animals. For genotyping, mouse tail DNA fragments were amplified by PCR using the following primers: F: 5'-GTCCAGACAGTTTCTAACTTTCATTC-3' and R: 5'-ATGTTTCAGTGTTCCAGAGGAACAGC-3'. PCR genotyping followed by HindIII digestion yielded 250 bp and 150 bp bands for homozygous δ-catenin G34S mice (G34S), 400 bp, 250 bp, and 150 bp bands for heterozygous δ-catenin G34S mice (HET), and a 400 bp band for WT (**Fig. S10b**). Each genotype was thus identified using PCR genotyping followed by HindIII digestion (**Fig. S10c**).

Generation of δ-catenin KO mice

δ-catenin KO mouse was developed in collaboration with Cyagen Biosciences Inc. utilizing the CRISPR-Cas9 technique (1). Cas9 mRNA and two single guide RNAs (sgRNAs) were microinjected into the C57Bl6/J zygotes, where sgRNAs directed Cas9 endonuclease to cleave within intron 1 and intron 2 of the mouse *δ-catenin* gene (**Fig. S11a**), yielding a double-strand break, which removed the exon 2 that contained the ATG initiation codon. The sgRNA sequences were 5'-GAGGGGGGAGAGGTCCGTTCTGG-3' and 5'-CTTCTTTAGGTGAACGTTGATGG-3' (the protospacer adjacent motif (PAM) sequences are underlined). Such breaks were repaired by non-homologous end joining, resulting in disruption of the *δ-catenin* gene expression *in vivo*. Cyagen Biosciences Inc. identified the optimal sequences for guide RNAs using the C57Bl6/J database to minimize off-target effects. sgRNAs that contain one or two-nucleotide mismatches to the DNA target in the 20-mer targeting region of the sgRNA do not function in the CRISPR-Cas9 system (2). We were unable to locate one or two base-mismatched sequences in the database for our sgRNAs, indicating that that δ-catenin KO was most likely successfully introduced without off-target effects. The founder mouse was crossed with WT C57Bl6/J mice to create heterozygous δ-catenin KO mice, which were subsequently used to make homozygous KO animals in the C57Bl6/J background. Each genotype was identified using PCR genotyping (**Fig. S11b**). For genotyping, mouse tail DNA fragments were amplified by PCR using the following primers: F1: 5'-TTAATCCATCGTGCTGCCAGTG-3', R1: 5'-CTCATCATAAGAAACACCTGGAAGG-3', and R2: 5'-CTCATACACATTCAGATTTAACCC-3'. PCR genotyping yielded a 675 bp band for homozygous δ-catenin KO mice (KO), 440 bp and 675 bp bands for heterozygous δ-catenin KO mice (HET), and a 440 bp band for WT (**Fig. S11b**). The animals used in the proposed research have been fully crossed to C57Bl6/J mice for more than eight generations and will be maintained on C57Bl6/J background. By immunoblotting whole brain tissues, we confirmed that our new δ-catenin KO mice did not express any full-length or truncated δ-catenin protein (**Fig. S11c**).

Immunoblotting

Immunoblotting was performed as described previously (3-18). Whole brains were rapidly removed and placed in ice-cold solution A (0.32 M sucrose, 1 mM $NaHCO_3$, 1 mM $MgCl_2$, and 0.5 mM $CaCl_2$) and protease inhibitors. The brains were subjected to dounce homogenization in 40 ml of solution A per 10 g of wet brain tissue. The homogenates were diluted to 10% weight/volume with solution A and centrifuged at 1,400 *g* for 10 min. The supernatant solution was saved as whole tissue lysates, and the pellet. Supernatants were then spun at 30,000 *g* for 15 min to obtain a crude P2 fraction. The pellet was resuspended in solution B (0.32 M sucrose and 1 mM $NaHCO_3$) using 24 ml of solution B per 10 g of starting material. This homogenate was layered on top of a 1 M sucrose and 1.2 M sucrose gradients and centrifuged at 82,500 *g* for 2 hr. Purified synaptosomes were collected at the 1 M and 1.2 M sucrose interface and were then collected by centrifugation at 48,200 *g* for

45 min. The pellets were resuspended in 25 mM This pH 8.4, and an equal volume of 1% Triton X-100 was added and rocked at 4°C for 30 min. These lysed synaptosomes were centrifuged at 32,800 *g* for 30 min. The PSD pellet was resuspended in 25mM This pH 8.4 with 2% SDS. Equal amounts of protein (whole cell lysates and PSD) were loaded on 10% SDS-PAGE gel and transferred to nitrocellulose membranes. Membranes were blotted with antibodies. The primary antibodies consisted of anti-δ-catenin (BD Biosciences, 1:1000 and Abcam, 1:1000), anti-GluA1 (Millipore, 1:2000), anti-GluA2 (Abcam, 1:2000), anti-pGSK3β (Cell Signaling Technology, 1:1000), and anti-actin (Abcam, 1:2000) antibodies. Protein bands were quantified using ImageJ (https://imagej.nih.gov/ij/).

Reagents

Proteasome inhibitor MG132 (Allfa Aesar) was used at 10 μM to treat SH-SY5Y cells 4 hours before collecting whole cell lysates. 2 mM lithium chloride (LiCl) (Sigma-Aldrich) was used to inhibit GSK3β activity in SH-SY5Y cells and cultured cortical neurons, and 2 mM sodium chloride (NaCl) (Sigma-Aldrich) was used as a control. 2 μM tetrodotoxin (TTX) (Abcam) was used to block spontaneous Ca^{2+} activity in cultured cortical neurons. 1 mM 4-methoxy-7-nitroindolinyl (MNI)-caged L-glutamate (Tocris Bioscience) was added to the culture media for glutamate uncaging. 20 μM 1-naphthyl acetyl spermine (NASPM) (abcam) was used to block CP-AMPARs.

GCaMP Ca^{2+} Imaging with glutamate uncaging

We carried out Ca^{2+} imaging with glutamate uncaging in cultured mouse cortical neurons to determine glutamatergic activity as described previously (19). For Ca^{2+} imaging, a genetically encoded Ca^{2+} indicator, GCaMP, was used. When AAVs of the same serotype are co-infected, many neurons are transduced by both viruses (20). We thus co-infected AAVs expressing CamK2a-Cre (Addgene #105558-AAV1), pENN.AAV.CamKII 0.4.Cre.SV40 was a gift from James M. Wilson (Addgene plasmid #105558 ; http://n2t.net/addgene:105558 ; RRID:Addgene_105558), and Cre-dependent GCaMP7s (Addgene #104495-AAV1) (21), pGP-AAV-CAG-FLEX-jGCaMP7s-WPRE was a gift from Douglas Kim & GENIE Project (Addgene plasmid # 104495 ; http://n2t.net/addgene:104495 ; RRID:Addgene_104495), in 4 days *in vitro* (DIV) neurons and imaged 12-13 DIV excitatory neurons. In addition, AAV expressing GCaMP6f under the control of the GABAergic neuron-specific enhancer of the mouse *Dlx* (mDlx) gene (Addgene #83899-AAV1) (22), pAAV-mDlx-GCaMP6f-Fishell-2 was a gift from Gordon Fishell (Addgene plasmid #83899-AAV1 ; http://n2t.net/addgene:83899 ; RRID:Addgene_83899), was infected in 4 DIV neurons and imaged 12-13 DIV inhibitory interneurons. Glass-bottom dishes were mounted on a temperature-controlled stage on an Olympus IX73 microscope and maintained at 37°C and 5% CO_2 using a Tokai-Hit heating stage and digital temperature and humidity controller. For glutamate uncaging, 1 mM 4-methoxy-7-nitroindolinyl (MNI)-caged L-glutamate was added to the culture media, and epi-illumination photolysis (390 nm, 0.12 mW/mm^2, 1 ms) was used to uncage glutamate in the whole field of view. 2 μM TTX was added to prevent action potential-dependent network activity. To block Ca^{2+}-permeable AMPA receptors, 20 μM NASPM was added to the culture media as described previously (10, 18). A baseline average of 20 frames (10 ms exposure for GCaMP7s and 50 ms exposure for GCaMP6f exposure) (F_0) were captured in the soma prior to glutamate uncaging, and 50 more frames were obtained after single photostimulation. The fractional change in fluorescence intensity relative to baseline ($\Delta F/F_0$) was calculated. The average peak amplitude in the control group was used to normalize the peak amplitude in each cell. The control group's average peak amplitude was compared to the experimental groups' average.

***In vitro* electrophysiology**

Whole-cell patch-clamp recordings of cortical neurons were performed similarly to that described before (23). In brief, neurons were patched in voltage-clamp mode using an internal solution containing (in mM) 135 $CsCl_2$, 1 EGTA, 1 NaGTP, 2 QX-314, and 10 HEPES-CsOH (pH 7.4, 310 mOsm). The extracellular solution contained (in mM) 140 NaCl, 5 KCl, 3 $CaCl_2$, 1 $MgCl_2$, 10 glucose, and 10 HEPES-NaOH (pH 7.4, 300 mOsm). AMPA receptor-mediated miniature excitatory postsynaptic currents (mEPSCs) were isolated by bath application of picrotoxin (100 μM, $GABA_A$ receptor/Glycine receptor blocker, Tocris Bioscience), CPP (50 μM, NMDA receptor inhibitor; Tocris Bioscience), and TTX (2 μM, Na^+-channel blocker, Ascent Scientific). All recordings were conducted at room temperature, and at a V_{hold} of -70 mV, using an integrated patch-clamp amplifier (IPA, Sutter Instruments) controlled by customized Igor Pro 8 (WaveMetrics) data acquisition system.

Three-chamber test

To determine social behaviors, a three-chamber test was performed with a modification of the previously described method (14). The test animals' interaction with strangers was determined by the reciprocal sniffing time as described previously (24, 25). The test animals' interaction with a novel object was determined by the sniffing time that was defined as each instance in which a test mouse's nose was oriented in a 10-degree head orientation and comes within 2 cm toward a mouse or a wire cup as described previously (26). Before the test session, the subject mouse was placed in the center chamber and allowed to habituate for 5 minutes. In the sociability test (10 minutes), an unfamiliar mouse (stranger 1) was placed in one side chamber under an inverted stainless-steel wire cup that allowed olfactory, visual, auditory, and tactile contacts, and an empty cup (a novel object) was placed in the opposite side chamber. During the social novelty test (10 minutes), a new unfamiliar mouse (stranger 2) was placed under a wire cup in the opposite side chamber that had been empty during the sociability phase. The subject mouse was allowed to explore freely in all 3 chambers during the tests. The behavior was recorded using a camera mounted overhead. The test animals' interaction with strangers was determined by the reciprocal sniffing time as described previously (24, 25). The test animals' interaction with a novel object was determined by the sniffing time that was defined as each instance in which a test mouse's nose was oriented in a 10-degree head orientation and comes within 2 cm toward a mouse or a wire cup as described previously (26). The discrimination index was calculated as (Total reciprocal sniffing time for stranger 1 – Total sniffing time for the object) / (Total reciprocal sniffing time for stranger 1 + Total sniffing time for the object) for the sociability test and (Total reciprocal sniffing time for stranger 2 – Total reciprocal sniffing time for stranger 1) / (Total reciprocal sniffing time for stranger 2 + Total reciprocal sniffing time for stranger 1) for the social novelty test. We confirmed the reciprocal sniffing time manually and blindly by two different investigators.

Buried food assay

The buried food assay was performed as described previously (5). Several days before the test, 2-3 Froot Loops (Kellogg's) were placed in each cage overnight to confirm that the food is palatable to the mice. Mice that did not consume the Froot Loops were omitted from the test. Mice were food-deprived for 24 hours prior to the test. 2 Froot Loops were placed in a clean cage and buried under fresh bedding prior to placing the mice in the cage. Mice were allowed 20 minutes to explore the cage searching for the hidden food and the latency to find and begin to nibble on the food was recorded. Mice that did not find the food after 20 minutes were excluded from the results. The latency was blindly scored by two different investigators.

Open field test

We measured locomotor activity and anxiety-like behavior using the open field test as carried out previously (14). The test mouse was first placed in the center of the open field chamber (40 W x 40 L x 40 H cm) for 5 minutes. Animals were then allowed to explore the chamber for 20 minutes. A 20 x 20 cm center square was defined as the inside zone. The behavior was recorded by a video camera. Data were analyzed using the ANY-maze tracking program to acquire total traveled distance (locomotor activity) and time spent outside and inside (anxiety-like behavior).

Figure S1. A schematic of N-cadherin-δ-catenin-ABP/GRIP-GluA2 synaptic complex.

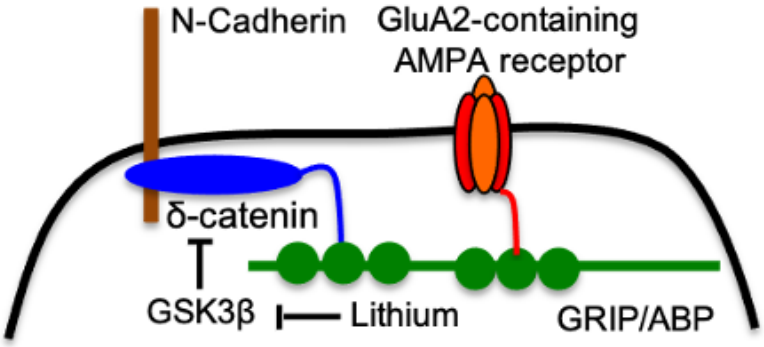

A schematic of N-cadherin-δ-catenin-ABP/GRIP-GluA2 synaptic complex and GSK3β regulation of δ-catenin. At PSD, δ-catenin interacts with N-cadherin, a synaptic cell adhesion protein. The carboxyl-terminus of δ-catenin binds to AMPA receptor-binding protein (ABP) and glutamate receptor-interacting protein (GRIP). This N-cadherin-δ-catenin-ABP/GRIP complex functions as an anchor for GluA2. GSK3β phosphorylates δ-catenin, which leads to δ-catenin degradation. The reduction of GSK3β activity by lithium stabilizes the N-cadherin-δ-catenin-ABP/GRIP-GluA2 complex.

Figure S2. Amino acid sequence homology between β-catenin, WT δ-catenin and G34S WT δ-catenin.

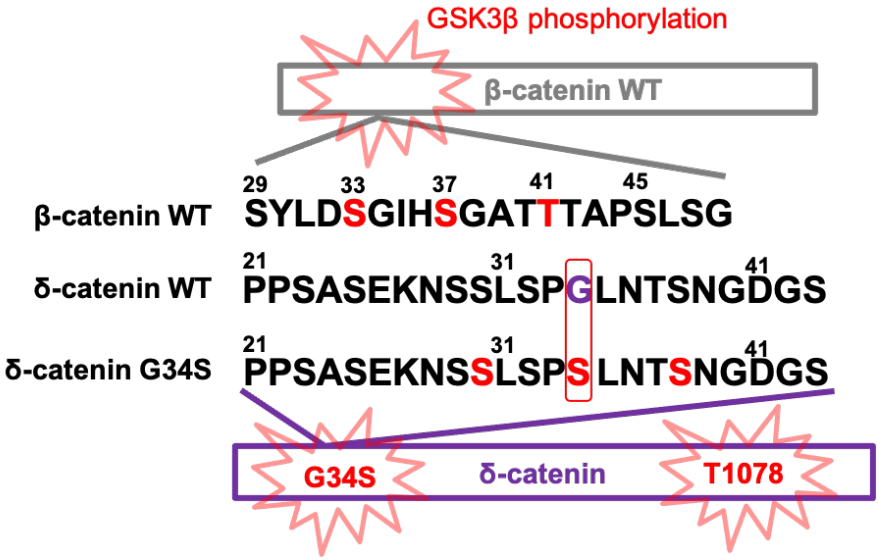

The δ-catenin G34S mutation adds an additional GSK3β-mediated phosphorylation site to induce δ-catenin degradation. GSK3β phosphorylation sites of β-catenin in the amino-terminal region known to induce proteasomal degradation of β-catenin highlighted in red (S33, S37, and T41) are comparable to possible GSK3β phosphorylation sites in the amino-terminus of G34S mutant δ-catenin also highlighted in red (S30, S34, and S38). In addition to GSK3β-mediated threonine 1078 phosphorylation site in the carboxyl-terminus of δ-catenin, these potential amino-terminal GSK3β-mediated phosphorylation sites may enhance δ-catenin degradation.

Figure S3. Proteasomal degradation enhances G34S δ-catenin degradation.

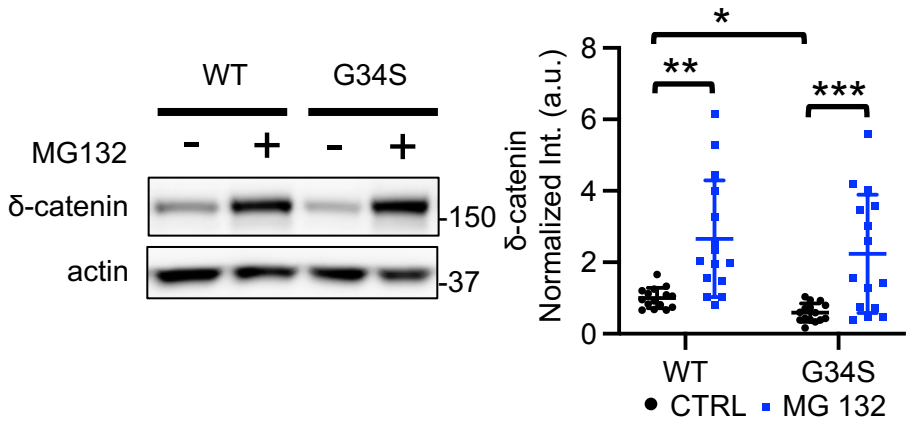

Representative immunoblots and summary graphs of normalized δ-catenin levels in SH-SY5Y cell lysates transfected with WT or G34S δ-catenin in the presence (+) or absence (-) of 10 μM MG132 (n = 15 immunoblots from 5 independent cultures, *$p < 0.05$, **$p < 0.01$, and ***$p < 0.001$, Kruskal-Wallis test with the Dunn's test). The position of molecular mass markers (kDa) is shown on the right of the blots. Mean ± SD.

Figure S4. Total δ-catenin and AMPAR levels in the cortex of WT and δ-catenin G34S mice.

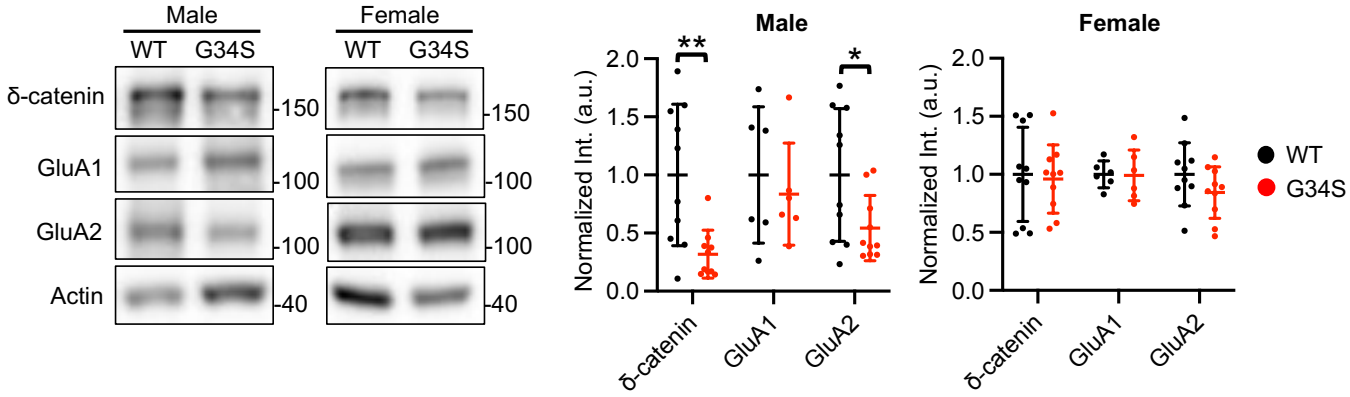

Representative immunoblots and summary graphs of normalized total δ-catenin, GluA1, and GluA2 levels in the male and female whole tissue lysates from the WT and δ-catenin G34S cortex (For δ-catenin and GluA2, n = 10 immunoblots from 4 mice in each condition. For GluA1, n = 6 immunoblots from 4 mice in each condition. *$p < 0.05$ and **$p < 0.01$, the unpaired two-tailed Student's t-test.). The position of molecular mass markers (kDa) is shown on the right of the blots. Mean ± SD.

Figure S5. Synaptic δ-catenin and AMPAR levels in the hippocampus of δ-catenin G34S and KO mice.

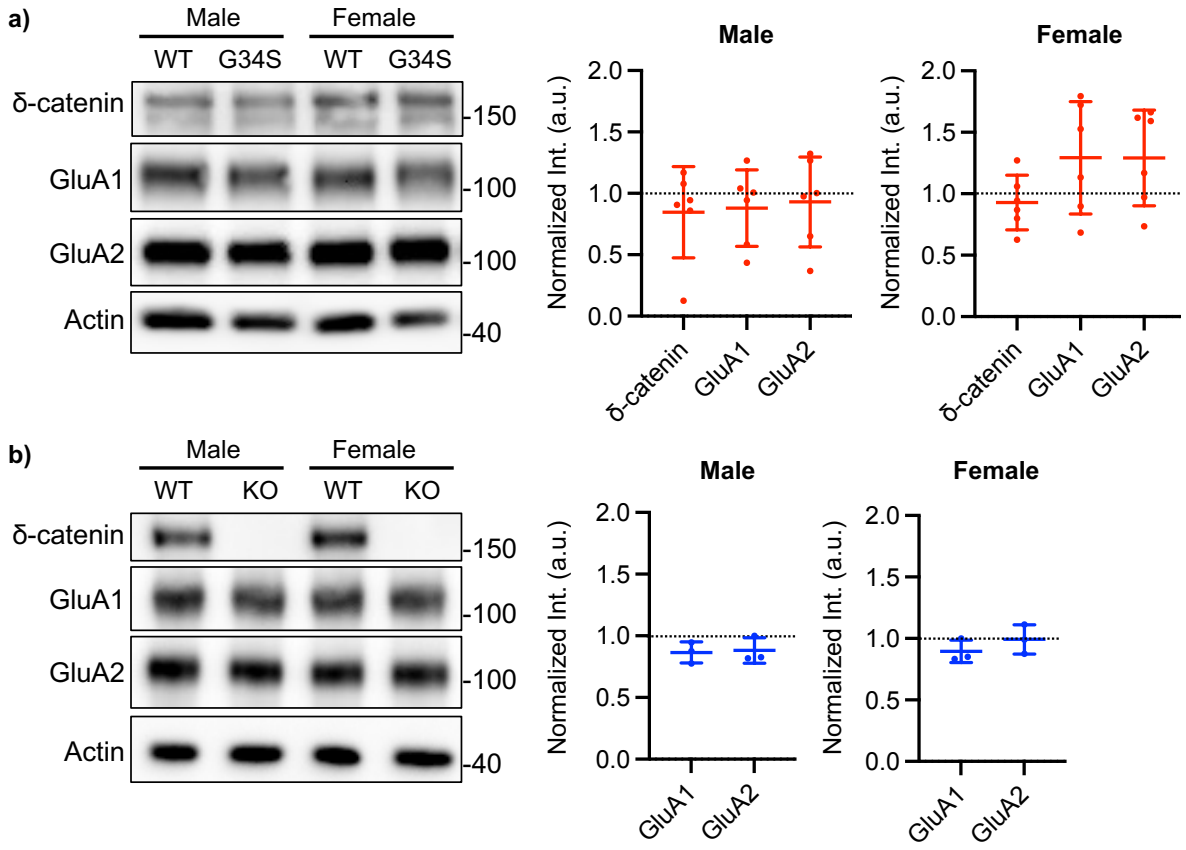

a) Representative immunoblots and summary graphs of normalized δ-catenin, GluA1, and GluA2 levels in the male and female hippocampal PSD fractions from the WT and G34S hippocampus (n = 6 immunoblots from 3 mice in each condition, Kruskal-Wallis test with the Dunn's test). **b)** Representative immunoblots and summary graphs of normalized GluA1 and GluA2 levels in the male and female hippocampal PSD fractions from the WT and KO hippocampus (n = 3 immunoblots from 3 mice in each condition, Kruskal-Wallis test with the Dunn's test). The position of molecular mass markers (kDa) is shown on the right of the blots. Mean ± SD.

Figure S6. Lithium treatment significantly reduces *in vivo* GSK3β activity.

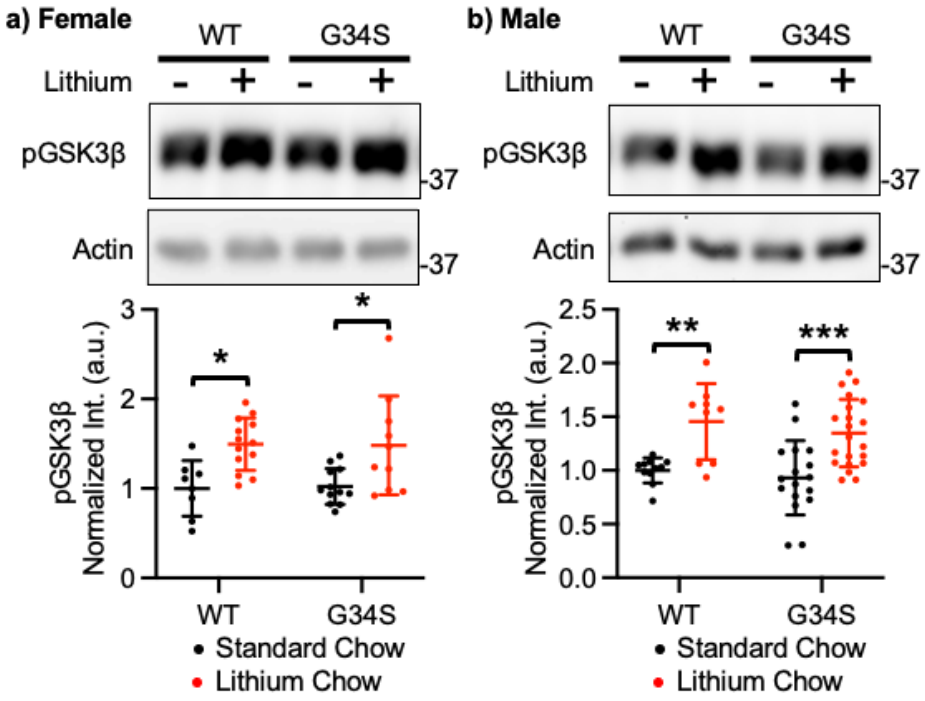

Representative immunoblots and summary graphs of normalized pGSK3β levels in the whole cell lysates from the cortex of standard chow (-) or lithium chow (+)-fed WT and δ-catenin G34S **a)** female (n=number of immunoblots [number of mice]. WT female + standard chow = 8 [6], WT female + lithium chow = 13 [6], G34S female + standard chow = 12 [6], and G34S female + lithium chow = 10 [6]) and **b)** male cortex (WT male + standard chow=11 [6], WT male + lithium chow = 9 [6], G34S male + standard chow = 17 [6], and G34S male + lithium chow = 21 [6]). *$p < 0.05$, **$p < 0.01$, and ***$p < 0.001$, Two-way ANOVA with the Tukey test). The position of molecular mass markers (kDa) is shown on the right of the blots. Mean ± SD.

Figure S7. Altered AMPAR-mediated glutamatergic activity in cultured δ-catenin G34S cortical neurons.

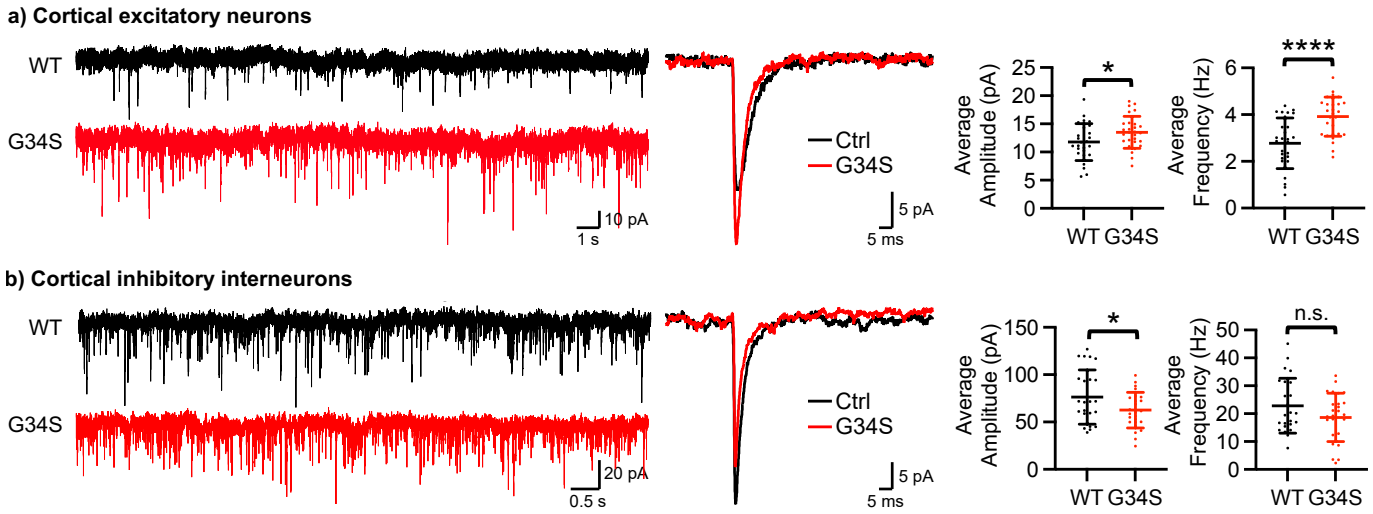

a) Representative (left) and average traces (superimposed, right) of mEPSCs and summary data of the average mEPSC amplitude and frequency in each condition in excitatory neurons (n = number of neurons from 2 independent cultures, WT = 28 and G34S = 28). **b)** Representative (left) and average traces (superimposed, right) of mEPSCs and summary data of the average mEPSC amplitude and frequency in each condition in inhibitory interneurons (n = number of neurons from 2 independent cultures, WT = 24 and G34S = 26, *p < 0.05 and ****p < 0.0001, the unpaired two-tailed Student's t-test). Mean ± SD.

Figure S8. Increased glutamatergic activity in cultured δ-catenin G34S cortical excitatory neurons is mediated by CP-AMPARs.

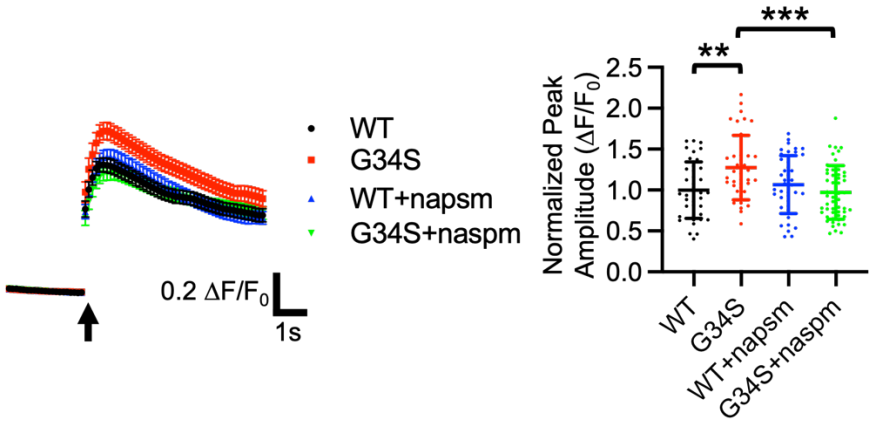

Average traces of GCaMP7s signals and summary data of normalized peak amplitude in each condition in excitatory neurons (n = number of neurons from 2 independent cultures, WT = 39, G34S = 38, WT + NASPM = 41, and G34S + NASPM = 54, $^{**}p < 0.01$ and $^{***}p < 0.01$, Two-way ANOVA with the Tukey test). An arrow indicates photostimulation. Mean ± SD.

Figure S9. Normal olfaction, locomotor activity, and anxiety levels in δ-catenin G34S and KO mice.

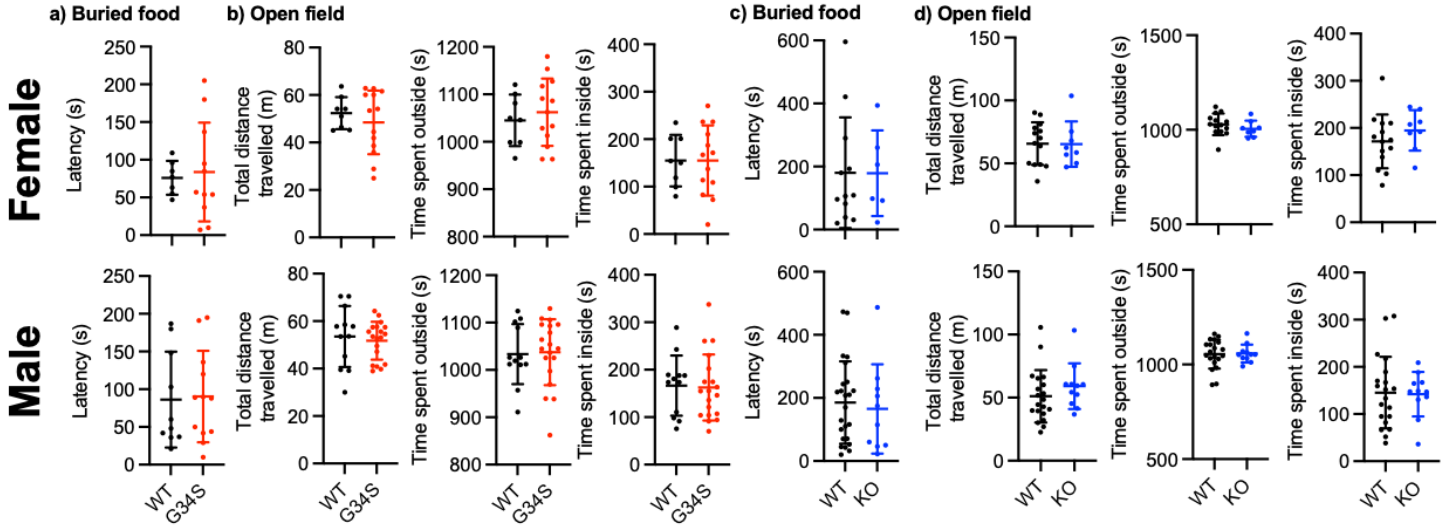

The results of the buried food test in **a)** females (n = 7 WT and 11 G34S mice) and males (n = 10 WT and 12 G34S mice). **b)** The results of the open field test measuring total distance travelled and time spent outside and inside females (n = 8 WT and 13 G34S mice) and males (n = 12 WT and 19 G34S mice). The results of the buried food test in **c)** females (n = 12 WT and 6 KO mice) and males (n = 24 WT and 10 KO mice). **d)** The results of the open field test measuring total distance travelled and time spent outside and inside in females (n = 18 WT and 8 KO mice) and males (n = 20 WT and 11 KO mice). Mean ± SD.

Figure S10. Generation of δ-catenin G34S mice.

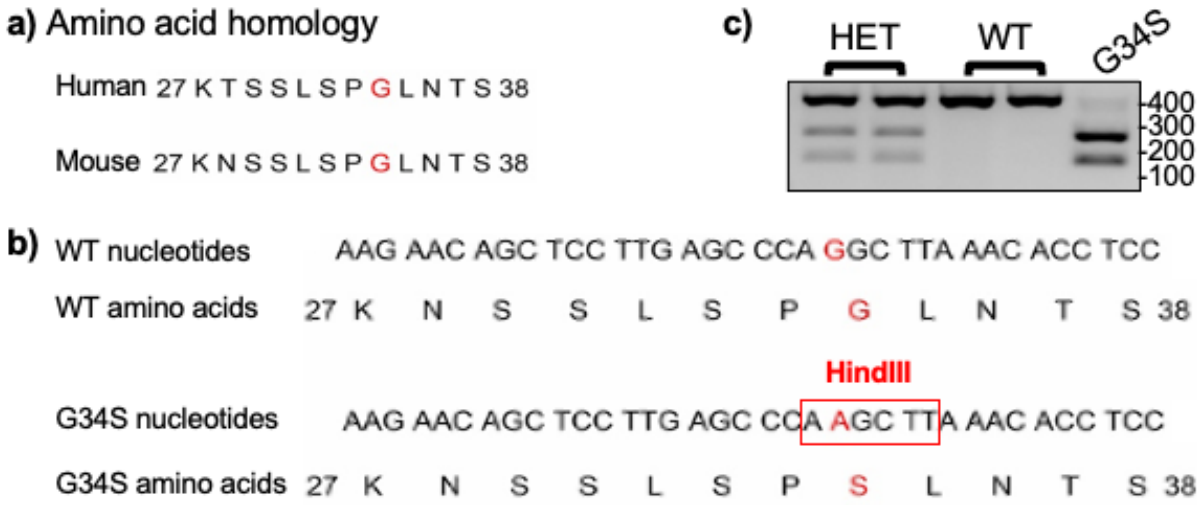

a) Amino acid sequence homology between human and mouse δ-catenin at indicated locus. **b)** Nucleotide sequence and corresponding amino acid sequence for WT and mutant alleles. The HindIII site is highlighted. **c)** For genotyping, mouse tail DNA fragments were amplified by PCR. PCR genotyping followed by HindIII digestion yields 250 bp and 150 bp bands for homozygous δ-catenin G34S mice (G34S), 400 bp, 250 bp, and 150 bp bands for heterozygous δ-catenin G34S mice (HET), and a 400 bp band for WT. The position of DNA size markers (bp) is shown on the right of the image.

Figure S11. Generation of δ-catenin KO mice.

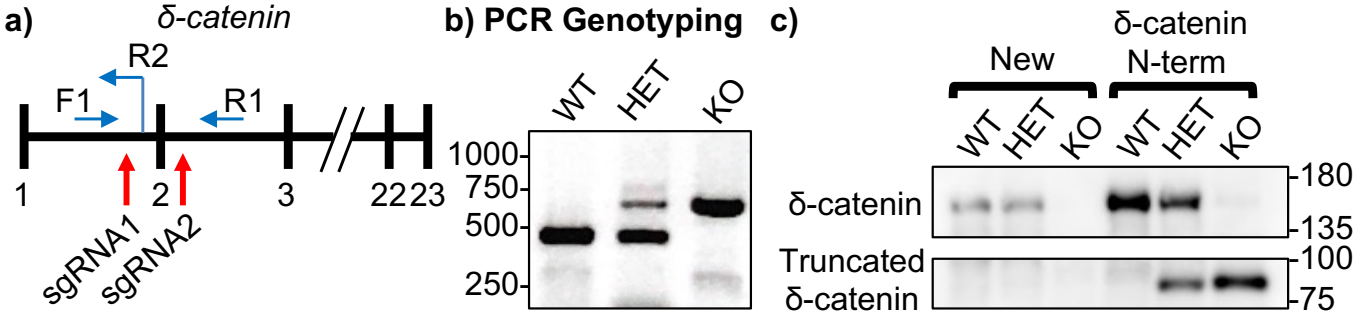

a) The strategy of generation of δ-catenin KO mice. The numbers indicate exons, red arrows indicate sgRNA target sites, and blue arrows indicate primers used for PCR genotyping. **b)** PCR genotyping yields a 675 bp band for homozygous δ-catenin KO mice (KO), 440 bp and 675 bp bands for heterozygous δ-catenin KO mice (HET), and a 440 bp band for WT. The position of DNA size markers (bp) is shown on the left of the image. **c)** Representative immunoblot images of δ-catenin levels in total cell lysates from the cortex of WT, HET, and KO mice of newly generated δ-catenin KO (New) and δ-catenin N-term animals showing that new δ-catenin KO mice have no full-length and truncated δ-catenin. The position of molecular mass markers (kDa) is shown on the right of the blots.

Table S1. Three-chamber test summary of WT and G34S mice with regular and lithium chow

Regular chow									
Female	WT (n = 11 mice)		G34S (n = 8 mice)		Male	WT (n = 11 mice)		G34S (n = 14 mice)	
Sociability	Stranger 1	Objective	Stranger 1	Objective	Sociability	Stranger 1	Objective	Stranger 1	Objective
Total Interaction Time (sec)	16.445 ± 4.244	10.855 ± 2.973	11.538 ± 3.387	13.513 ± 3.433	Total Interaction Time (sec)	16.864 ± 5.169	8.655 ± 3.244	10.986 ± 4.035	10.829 ± 2.691
	Stranger 1 vs. Objective, $p = 0.0042$		Stranger 1 vs. Objective, $p = 0.3888$			Stranger 1 vs. Objective, $p < 0.0001$		Stranger 1 vs. Objective, $p = 0.9995$	
	WT Stranger 1 vs. G34S Stranger 1, $p = 0.0268$					WT Stranger 1 vs. G34S Stranger 1, $p = 0.0023$			
Social novelty	Stranger 1	Stranger 2	Stranger 1	Stranger 2	Social novelty	Stranger 1	Stranger 2	Stranger 1	Stranger 2
Total Interaction Time (sec)	6.182 ± 1.795	12.827 ± 4.303	6.825 ± 2.712	8.425 ± 2.843	Total Interaction Time (sec)	7.391 ± 3.428	17.573 ± 4.037	7.679 ± 9.314	9.314 ± 5.332
	Stranger 1 vs. 2, $p < 0.0001$		Stranger 1 vs. 2, $p = 0.7307$			Stranger 1 vs. 2, $p < 0.0001$		Stranger 1 vs. 2, $p = 0.7297$	
	WT Stranger 2 vs. G34S Stranger 2, $p = 0.0212$					WT Stranger 2 vs. G34S Stranger 2, $p < 0.0001$			
Lithium chow									
Female	WT (n = 13 mice)		G34S (n = 9 mice)		Male	WT (n = 8 mice)		G34S (n = 12 mice)	
Sociability	Stranger 1	Objective	Stranger 1	Objective	Sociability	Stranger 1	Objective	Stranger 1	Objective
Total Interaction Time (sec)	36.192 ± 14.596	15.069 ± 7.317	31.800 ± 14.691	13.544 ± 4.571	Total Interaction Time (sec)	32.850 ± 12.862	15.500 ± 9.699	28.042 ± 10.979	16.667 ± 7.563
	Stranger 1 vs. Objective, $p = 0.0001$		Stranger 1 vs. Objective, $p = 0.0074$			Stranger 1 vs. Objective, $p = 0.0089$		Stranger 1 vs. Objective, $p = 0.0468$	
	WT Stranger 1 vs. G34S Stranger 1, $p = 0.8061$					WT Stranger 1 vs. G34S Stranger 1, $p = 0.7336$			
Social novelty	Stranger 1	Stranger 2	Stranger 1	Stranger 2	Social novelty	Stranger 1	Stranger 2	Stranger 1	Stranger 2
Total Interaction Time (sec)	8.746 ± 3.242	33.154 ± 19.031	10.433 ± 7.117	35.989 ± 13.988	Total Interaction Time (sec)	7.363 ± 3.864	18.800 ± 12.404	8.450 ± 4.345	17.258 ± 5.579
	Stranger 1 vs. 2, $p < 0.0001$		Stranger 1 vs. 2, $p = 0.0006$			Stranger 1 vs. 2, $p = 0.0117$		Stranger 1 vs. 2, $p = 0.0182$	
	WT Stranger 2 vs. G34S Stranger 2, $p = 0.9550$					WT Stranger 2 vs. G34S Stranger 2, $p = 0.9615$			

Table S2. The discrimination index of WT and G34S mice with regular and lithium chow

Female	Regular chow		Lithium chow		Male	Regular chow		Lithium chow	
	WT	G34S	WT	G34S		WT	G34S	WT	G34S
Sociability Discrimination index	0.203 ± 0.126	-0.087 ± 0.128	0.401 ± 0.150	0.383 ± 0.081	Sociability Discrimination index	0.323 ± 0.201	-0.014 ± 0.226	0.389 ± 0.131	0.267 ± 0.147
	WT vs. G34S, $p = 0.0001$		WT vs. G34S, $p = 0.9868$			WT vs. G34S, $p = 0.0003$		WT vs. G34S, $p = 0.4847$	
	G34S regular chow vs. G34S lithium, $p < 0.0001$					G34S regular chow vs. G34S lithium, $p = 0.0024$			
Social Novelty Discrimination index	0.341 ± 0.091	0.107 ± 0.134	0.532 ± 0.166	0.548 ± 0.227	Social Novelty Discrimination index	0.423 ± 0.208	0.015 ± 0.290	0.424 ± 0.262	0.379 ± 0.171
	WT vs. G34S, $p = 0.0168$		WT vs. G34S, $p = 0.9954$			WT vs. G34S, $p = 0.0115$		WT vs. G34S, $p = 0.0115$	
	G34S regular chow vs. G34S lithium, $p < 0.0001$					G34S regular chow vs. G34S lithium, $p = 0.0372$			

Table S3. Summary of the buried food and open field tests

	Buried food test	Open field test		
Female	The latency (Seconds)	Total distance travelled (m)	Total time spent outside (Seconds)	Total time spent inside (Seconds)
WT	76.000 ± 22.443	52.378 ± 6.751	1045.150 ± 54.380	154.850 ± 54.380
G34S	83.727 ± 65.521	48.454 ± 13.409	1062.338 ± 70.804	154.892 ± 73.942
	p = 0.7694	p = 0.4537	p = 0.5645	p = 0.9988
Male	The latency (Seconds)	Total distance travelled (m)	Total time spent outside (Seconds)	Total time spent inside (Seconds)
WT	86.200 ± 63.554	53.532 ± 12.868	1033.308 ± 63.382	166.692 ± 63.382
G34S	90.333 ± 60.593	51.742 ± 7.954	1037.368 ± 69.715	162.632 ± 69.715
	p = 0.8777	p = 0.6346	p = 0.8713	p = 0.8623
	Buried food test	Open field test		
Female	The latency (Seconds)	Total distance travelled (m)	Total time spent outside (Seconds)	Total time spent inside (Seconds)
WT	180.250 ± 175.360	65.701 ± 16.926	1028.536 ± 57.074	171.464 ± 57.074
KO	178.833 ± 135.632	65.285 ± 18.005	1005.225 ± 42.884	194.775 ± 42.884
	p = 0.9864	p = 0.9573	p = 0.3288	p = 0.3288
Male	The latency (Seconds)	Total distance travelled (m)	Total time spent outside (Seconds)	Total time spent inside (Seconds)
WT	185.542 ± 130.374	51.071 ± 20.755	1054.510 ± 75.972	145.490 ± 75.972
KO	165.200 ± 141.551	59.102 ± 18.124	1057.845 ± 47.091	142.155 ± 47.091
	p = 0.6885	p = 0.2909	p = 0.8961	p = 0.8961

Table S4. Three-chamber test summary of WT and KO mice.

Regular chow									
Female	WT (n = 16 mice)		KO (n = 14 mice)		Male	WT (n = 20 mice)		KO (n = 15 mice)	
Sociability	Stranger 1	Objective	Stranger 1	Objective	Sociability	Stranger 1	Objective	Stranger 1	Objective
Total Interaction Time (sec)	16.981 ± 8.908	8.731 ± 3.853	9.393 ± 5.173	9.829 ± 2.496	Total Interaction Time (sec)	19.225 ± 12.543	8.290 ± 4.968	11.053 ± 6.531	9.840 ± 3.052
	Stranger 1 vs. Objective, $p = 0.0008$		Stranger 1 vs. Objective, $p = 0.9971$			Stranger 1 vs. Objective, $p = 0.0003$		Stranger 1 vs. Objective, $p = 0.9753$	
	WT Stranger 1 vs. KO Stranger 1, $p = 0.0035$					WT Stranger 1 vs. KO Stranger 1, $p = 0.0192$			
Social novelty	Stranger 1	Stranger 2	Stranger 1	Stranger 2	Social novelty	Stranger 1	Stranger 2	Stranger 1	Stranger 2
Total Interaction Time (sec)	3.488 ± 3.466	16.994 ± 10.683	4.293 ± 4.296	7.221 ± 5.148	Total Interaction Time (sec)	3.670 ± 2.497	20.880 ± 11.455	6.713 ± 5.899	9.380 ± 4.679
	Stranger 1 vs. 2, $p < 0.0001$		Stranger 1 vs. 2, $p = 0.6511$			Stranger 1 vs. 2, $p < 0.0001$		Stranger 1 vs. 2, $p = 0.7403$	
	WT Stranger 2 vs. KO Stranger 2, $p = 0.0010$					WT Stranger 2 vs. KO Stranger 2, $p < 0.0001$			

Table S5. The discrimination index of WT and KO mice

Regular chow					
Female	WT	KO	Male	WT	KO
Sociability Discrimination index	0.307 ± 0.150	-0.081 ± 0.373	Sociability Discrimination index	0.360 ± 0.195	-0.011 ± 0.408
	p = 0.0007			p = 0.0010	
Social Novelty Discrimination index	0.676 ± 0.222	0.322 ± 0.405	Social Novelty Discrimination index	0.657 ± 0.232	0.255 ± 0.412
	p = 0.0053			p = 0.0009	

Table S6. Three-chamber test summary of G34S and KO mice with lithium chow.

Lithium chow									
Female	G34S (n = 9 mice)		KO (n = 7 mice)		Male	G34S (n = 12 mice)		KO (n = 7 mice)	
Sociability	Stranger 1	Objective	Stranger 1	Objective	Sociability	Stranger 1	Objective	Stranger 1	Objective
Total Interaction Time (sec)	31.800 ± 14.691	31.800 ± 14.691	13.200 ± 5.026	13.571 ± 4.549	Total Interaction Time (sec)	28.042 ± 10.979	16.667 ± 7.563	17.771 ± 2.906	13.457 ± 3.363
	Stranger 1 vs. Objective, $p = 0.0008$		Stranger 1 vs. Objective, $p = 0.9998$			Stranger 1 vs. Objective, $p = 0.0058$		Stranger 1 vs. Objective, $p = 0.7312$	
	WT Stranger 1 vs. G34S Stranger 1, $p = 0.0014$					WT Stranger 1 vs. G34S Stranger 1, $p = 0.0431$			
Social novelty	Stranger 1	Stranger 2	Stranger 1	Stranger 2	Social novelty	Stranger 1	Stranger 2	Stranger 1	Stranger 2
Total Interaction Time (sec)	10.433 ± 7.117	35.989 ± 13.988	15.371 ± 6.336	20.500 ± 6.562	Total Interaction Time (sec)	8.958 ± 4.248	16.650 ± 5.767	14.443 ± 6.724	17.300 ± 3.818
	Stranger 1 vs. 2, $p < 0.0001$		Stranger 1 vs. 2, $p = 0.7383$			Stranger 1 vs. 2, $p = 0.0011$		Stranger 1 vs. 2, $p = 0.7310$	
	WT Stranger 2 vs. G34S Stranger 2, $p = 0.0142$					WT Stranger 2 vs. G34S Stranger 2, $p > 0.9999$			

Table S7. The discrimination index of G34S and KO mice with lithium chow

Lithium chow					
Female	G34S	KO	Male	G34S	KO
Sociability Discrimination index	0.382 ± 0.081	-0.017 ± 0.130	Sociability Discrimination index	0.267 ± 0.147	0.111 ± 0.102
	$p < 0.0001$			$p = 0.0247$	
Social Novelty Discrimination index	0.549 ± 0.228	0.147 ± 0.304	Social Novelty Discrimination index	0.379 ± 0.171	0.116 ± 0.168
	$p = 0.0090$			$p = 0.0046$	

References

1. D. W. Harms *et al.*, Mouse Genome Editing Using the CRISPR/Cas System. *Curr Protoc Hum Genet* **83**, 15 17 11-27 (2014).
2. E. M. Anderson *et al.*, Systematic analysis of CRISPR-Cas9 mismatch tolerance reveals low levels of off-target activity. *J Biotechnol* **211**, 56-65 (2015).
3. M. Farooq *et al.*, Lithium increases synaptic GluA2 in hippocampal neurons by elevating the delta-catenin protein. *Neuropharmacology* 10.1016/j.neuropharm.2016.10.025 (2016).
4. S. Kim, A. N. Lapham, C. G. Freedman, T. L. Reed, W. K. Schmidt, Yeast as a tractable genetic system for functional studies of the insulin-degrading enzyme. *The Journal of biological chemistry* **280**, 27481-27490 (2005).
5. S. Kim *et al.*, Brain region-specific effects of cGMP-dependent kinase II knockout on AMPA receptor trafficking and animal behavior. *Learning & memory* **23**, 435-441 (2016).
6. S. Kim *et al.*, Evidence that the rab5 effector APPL1 mediates APP-betaCTF-induced dysfunction of endosomes in Down syndrome and Alzheimer's disease. *Molecular psychiatry* 10.1038/mp.2015.97 (2015).
7. S. Kim, J. Shou, S. Abera, E. B. Ziff, Sucrose withdrawal induces depression and anxiety-like behavior by Kir2.1 upregulation in the nucleus accumbens. *Neuropharmacology* **130**, 10-17 (2018).
8. S. Kim *et al.*, Network compensation of cyclic GMP-dependent protein kinase II knockout in the hippocampus by Ca2+-permeable AMPA receptors. *Proc Natl Acad Sci U S A* **112**, 3122-3127 (2015).
9. S. Kim, C. J. Violette, E. B. Ziff, Reduction of increased calcineurin activity rescues impaired homeostatic synaptic plasticity in presenilin 1 M146V mutant. *Neurobiol Aging* **36**, 3239-3246 (2015).
10. S. Kim, E. B. Ziff, Calcineurin mediates synaptic scaling via synaptic trafficking of Ca2+-permeable AMPA receptors. *PLoS biology* **12**, e1001900 (2014).
11. J. P. Roberts, S. A. Stokoe, M. F. Sathler, R. A. Nichols, S. Kim, Selective co-activation of alpha7- and alpha4beta2-nicotinic acetylcholine receptors reverses beta-amyloid-induced synaptic dysfunction. *The Journal of biological chemistry* 10.1016/j.jbc.2021.100402, 100402 (2021).
12. M. F. Sathler *et al.*, HIV and FIV glycoproteins increase cellular tau pathology via cGMP-dependent kinase II activation. *Journal of cell science* **135** (2022).
13. M. F. Sathler *et al.*, Phosphorylation of the AMPA receptor subunit GluA1 regulates clathrin-mediated receptor internalization. *Journal of cell science* **134** (2021).
14. J. Shou, A. Tran, N. Snyder, E. Bleem, S. Kim, Distinct Roles of GluA2-lacking AMPA Receptor Expression in Dopamine D1 or D2 Receptor Neurons in Animal Behavior. *Neuroscience* **398**, 102-112 (2018).
15. J. L. Sun *et al.*, Co-activation of selective nicotinic acetylcholine receptors is required to reverse beta amyloid-induced Ca(2+) hyperexcitation. *Neurobiol Aging* **84**, 166-177 (2019).
16. K. Sztukowski *et al.*, HIV induces synaptic hyperexcitation via cGMP-dependent protein kinase II activation in the FIV infection model. *PLoS biology* **16**, e2005315 (2018).
17. T. M. Tran *et al.*, Loss of cGMP-dependent protein kinase II alters ultrasonic vocalizations in mice, a model for speech impairment in human microdeletion 4q21 syndrome. *Neuroscience letters* **759**, 136048 (2021).
18. A. Zaytseva *et al.*, Ketamine’s rapid antidepressant effects are mediated by Ca²⁺-permeable AMPA receptors in the hippocampus. *bioRxiv* 10.1101/2022.12.05.519102, 2022.2012.2005.519102 (2023).
19. A. Zaytseva *et al.*, Ketamine’s rapid antidepressant effects are mediated by Ca²⁺-permeable AMPA receptors in the hippocampus. *bioRxiv* 10.1101/2022.12.05.519102, 2022.2012.2005.519102 (2022).
20. J. Y. Kim *et al.*, Viral transduction of the neonatal brain delivers controllable genetic mosaicism for visualising and manipulating neuronal circuits in vivo. *The European journal of neuroscience* **37**, 1203-1220 (2013).
21. H. Dana *et al.*, High-performance calcium sensors for imaging activity in neuronal populations and microcompartments. *Nature methods* **16**, 649-657 (2019).
22. J. Dimidschstein *et al.*, A viral strategy for targeting and manipulating interneurons across vertebrate species. *Nat Neurosci* **19**, 1743-1749 (2016).
23. S. R. Burlingham *et al.*, Induction of synapse formation by de novo neurotransmitter synthesis. *Nat Commun* **13**, 3060 (2022).

24. S. Kim *et al.*, Neural circuit pathology driven by Shank3 mutation disrupts social behaviors. *Cell Rep* **39**, 110906 (2022).
25. S. Kim, Y. E. Kim, I. H. Kim, Simultaneous analysis of social behaviors and neural responses in mice using round social arena system. *STAR Protoc* **3**, 101722 (2022).
26. W. Cao *et al.*, Gamma Oscillation Dysfunction in mPFC Leads to Social Deficits in Neuroligin 3 R451C Knockin Mice. *Neuron* **97**, 1253-1260 e1257 (2018).